



Proceedings of the
Estonian Academy of Sciences
2025, 74, 2, 109–114

<https://doi.org/10.3176/proc.2025.2.04>

www.eap.ee/proceedings
Estonian Academy Publishers

SOLID MECHANICS

RESEARCH ARTICLE

Received 31 January 2025
Accepted 24 February 2025
Available online 27 March 2025

Keywords:

functionally graded materials,
sandwich beam, TPMS core

Corresponding author:

Caner Solar
canersolar54@trakya.edu.tr

Citation:

Solar, C., Demirhan, P. A. and Taskin, V.
2025. Investigation of static behavior of
functionally graded porous sandwich
beams with TPMS core. *Proceedings of
the Estonian Academy of Sciences*,
74(2), 109–114.
<https://doi.org/10.3176/proc.2025.2.04>

Investigation of static behavior of functionally graded porous sandwich beams with TPMS core

Caner Solar, Pinar Aydan Demirhan and Vedat Taskin

Department of Mechanical Engineering, Trakya University, Edirne, Turkey

ABSTRACT

Functionally graded materials (FGMs) are innovative structures created by combining the properties of different materials. Functionally graded porous materials (FGPMs) are materials in which the size, shape, distribution, and density of pores change gradually in a specific direction, providing lightness and high energy absorption. Triply periodic minimal surface (TPMS) structures, especially when used in the inner layers, optimize load distribution and energy absorption characteristics. In this study, bending analyses of a simply supported functionally graded porous sandwich beam were performed. The surface layers of the beam consist of an isotropic material, while the core layer is made of a functionally graded TPMS structure. In this study, it is assumed that the material properties of the functionally graded porous surface and core layers vary according to the force law distribution along the thickness. The equations of motion of the beam were derived using Hamilton's principle. Solutions were obtained in closed form using the Navier method. Numerical results were obtained by varying the density and the volume fraction index, the thickness-to-length ratio, and the thickness ratios of the core and surface layers.

1. Introduction

Functionally graded materials (FGMs) are advanced structures that seamlessly integrate the properties of different materials, offering tailored mechanical and structural advantages. In particular, functionally graded porous materials (FGPMs) enhance lightness and energy absorption by varying the size, shape, and distribution of pores in a specific direction (Demirhan and Taskin 2019). When combined with triply periodic minimal surface (TPMS) structures in the inner layers, these materials optimize load distribution and energy absorption, making them ideal for innovative engineering applications. Recent studies have further explored various aspects of TPMS structures to understand their unique mechanical and dynamic behaviors. For instance, Kurup and Pitchaimani (2023) explored the aeroelastic flutter characteristics of functionally graded TPMS beams, highlighting their unique dynamic behavior. Qiu et al. (2025) conducted an in-depth analysis of the energy dissipation characteristics of sand-filled TPMS lattices under cyclic loading, providing significant insights into their structural resilience. Similarly, Egeh et al. (2022) focused on the flexural properties of functionally graded and hybridized AlSi10Mg TPMS latticed beams, showcasing the potential of these materials for load-bearing applications. Tran et al. (2024) presented a groundbreaking investigation of three novel computational modeling frameworks tailored for graphene platelet-reinforced functionally graded TPMS (GPLR-FG-TPMS) plates. Nguyen-Xuan et al. (2023) complemented this research by modeling FG-TPMS plates to evaluate their performance under varying conditions. Viet et al. (2022) extended the scope by examining the mechanical properties and wave propagation characteristics of TPMS lattice structures. Finally, Lin et al. (2022) investigated the sound insulation capacities of TPMS sandwich panels, employing theoretical, numerical, and experimental approaches to emphasize their acoustic benefits.

In this study, the material properties of the functionally graded porous surface and core layers are assumed to vary according to the force law distribution along the thickness. The equations of motion were derived using Hamilton's principle, and closed-form solutions were obtained via the Navier

method. Numerical analyses were conducted by varying parameters such as porosity coefficient, thickness-to-length ratio, and the thickness ratios of the core and surface layers. In the literature, no previous studies have presented results for TPMS-based beams. The results for TPMS-based beams are presented for the first time in this study.

2. Basic equations and assumptions

In this study, FG-TPMS sandwich beams were analyzed. Among sheet-based architectural designs, the gyroid model was selected and examined (Fig. 1). The mathematical representations of this model are provided in Eqs (1) and (2) (Nguyen-Xuan et al. 2023).

$$\text{Gyroid: } -t \leq \sin(\omega_1 x) \cos(\omega_2 y) + \sin(\omega_2 y) \cos(\omega_3 z) + \sin(\omega_3 z) \cos(\omega_1 x) \leq t, \quad (1)$$

$$\omega_i = \frac{2\pi n_i}{l_i}, \quad i = 1, 2, 3, \quad (2)$$

where t is the TPMS control parameter, n_i is the quantity of unit cells and l_i is the length.

In this study, the density of the functionally graded TPMS structure is assumed to vary in a single pattern: symmetric. Additionally, an approach based on these patterns is used for the variation of the density of the sandwich structure.

For sandwich plates:

$$\rho = (\rho_{max} - \rho_{min}) \times V_A(z) + \rho_{min}, \quad \rho = (\rho_{max} - \rho_{min}) \times V_B(z) + \rho_{min}. \quad (3)$$

ρ_{max} and ρ_{min} represent the highest and the lowest densities of the structure, respectively. $V(z)$ is the volume fraction function, defined as follows:

$$V_A(z) = \begin{cases} 0 & h_1 \leq z \leq h_2 \\ \left(\frac{z-h_2}{h_3-h_2}\right)^n & h_2 < z \leq h_3 \\ 1 & h_3 < z \leq h_4 \end{cases}, \quad V_B(z) = \begin{cases} 0 & h_1 \leq z \leq h_2 \\ \left(1 - \cos\left(\frac{\pi z}{h_3-h_2}\right)\right)^n & h_2 < z \leq h_3 \\ 1 & h_3 < z \leq h_4 \end{cases}. \quad (4)$$

The mechanical properties of the FG-TPMS plates (Table 2) are characterized using the two-phase fitting method introduced by Nguyen-Xuan et al. (2023).

In Table 1, the relative elasticity modulus, relative shear modulus, and Poisson's ratio of the TPMS structures are expressed as functions of density. For the FG-TPMS sandwich structures given in Eqs (3) and (4), it is assumed that the upper and lower surface layers are isotropic. As a result, the elasticity modulus, shear modulus, and Poisson's ratio remain constant in these layers due to the constant density. However, within the FG-TPMS core of the sandwich structures, these properties vary with density across the thickness.

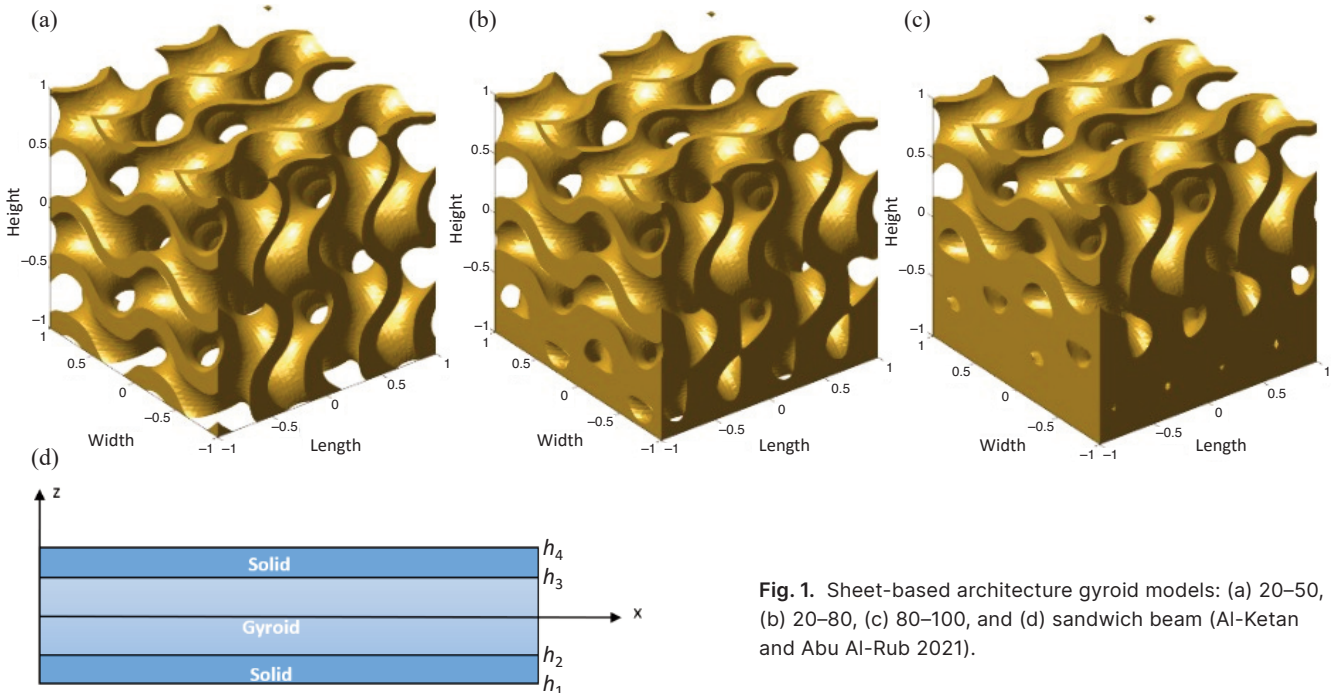


Fig. 1. Sheet-based architecture gyroid models: (a) 20–50, (b) 20–80, (c) 80–100, and (d) sandwich beam (Al-Ketan and Abu Al-Rub 2021).

Table 1. Layer types and height values of h_1, h_2, h_3, h_4

Layer types	h_1	h_2	h_3	h_4
1-8-1	$-h/2$	$-2h/5$	$2h/5$	$h/2$
1-2-1	$-h/2$	$-h/4$	$h/4$	$h/2$
2-1-2	$-h/2$	$-h/10$	$h/10$	$h/2$

Table 2. Mechanical properties of sheet-based TPMS structures

Gyroid (G)	$\frac{E}{E_s} = \begin{cases} 0.596\rho^{1.467} \\ 0.962\rho^{2.351} + 0.038 \end{cases}$	$\begin{cases} \rho \leq 0.45 \\ \rho > 0.45 \end{cases}$
	$\frac{G}{G_s} = \begin{cases} 0.777\rho^{1.544} \\ 0.973\rho^{1.982} + 0.027 \end{cases}$	$\begin{cases} \rho \leq 0.45 \\ \rho > 0.45 \end{cases}$
	$\nu = \begin{cases} 0.192e^{-1.349\rho} + 0.202 \\ 0.402\rho^2 - 0.603\rho + 0.501 \end{cases}$	$\begin{cases} \rho \leq 0.50 \\ \rho > 0.50 \end{cases}$

Table 3. Maximum and minimum values of the density and volume fraction exponents for the three cases

Pattern	Case	ρ_{\min}	ρ_{\max}	n	Pattern	Case	ρ_{\min}	ρ_{\max}	n
A	A1	0.20	0.5	1.0	B	B1	0.20	0.5	0.561
	A2	0.20	0.8	3.0		B2	0.20	0.8	1.757
	A3	0.25	1.0	6.5		B3	0.25	1.0	3.943

The hyperbolic shear deformation beam theory is a framework developed to analyze the mechanical behavior of planar sandwich structures. This theory aims to provide more accurate results by properly accounting for the shear stresses on the upper and lower surfaces of the beam.

The displacement field of the hyperbolic shear deformation beam theory is expressed in Eqs (5) and (6):

$$u(x, z) = u_0(x) - \frac{zdw_0}{dx} + f\phi(x),$$

$$w(x) = w_0(x), \tag{5}$$

$$f = [z \cosh(1/2) - h \sin(z/h)], \quad g = f' = [\cosh(1/2) - \cos(z/h)]. \tag{6}$$

According to the hyperbolic shear deformation beam theory, the non-zero normal (ϵ_x) and shear (γ_{zx}) strains at any point of the beam are related to the unknown displacement variables $\epsilon_x^0, k_x^b, k_x^s, \gamma_{zx}^0$ as expressed in Eqs (7) and (8), and occur at the points where they are related as follows:

$$\epsilon_x = \epsilon_x^0 + zk_x^b + fk_x^s, \quad \gamma_{zx} = g\gamma_{zx}^0, \tag{7}$$

$$\epsilon_x^0 = \frac{du_0}{dx}, \quad k_x^b = -\frac{d^2w_0}{dx^2}, \quad k_x^s = \frac{d\phi}{dx}, \quad \gamma_{xz}^0 = 0. \tag{8}$$

The stress-strain relationship at any point in the k layer of the beam is given by the one-dimensional Hooke's law in Eq. (9):

$$\sigma_x^k = E^k(z)\epsilon_x^k, \quad \tau_{xz}^k = G^k(z)\gamma_{zx}^k, \quad G^k(z) = \frac{E^k(z)}{2(1+\nu)}. \tag{9}$$

The equations of motion for the FG sandwich beam based on the hyperbolic shear deformation theory are derived using Hamilton's principle. In FG sandwich beams, Hamilton's principle serves as the fundamental principle for deriving the equations of motion, expressing the condition where variations in the total energy of the system are zero:

$$\int_{t_1}^{t_2} (\delta U - \delta V + \delta K) dt = 0. \tag{10}$$

The change in the strain of energy is expressed by Eq. (11):

$$\delta U = \int_0^L \int_{-\frac{b}{2}}^{\frac{b}{2}} \int_{-\frac{h}{2}}^{\frac{h}{2}} (\sigma_x^k \delta \varepsilon_x + \tau_{zx}^k \delta \gamma_{zx}) dz dy dx = \int_0^L \left(N_x \frac{d\delta u_0}{dx} - M^c \frac{d^2 \delta w_0}{dx^2} + M^s \frac{d^2 \delta \phi}{dx^2} + Q \delta \phi \right) dx. \quad (11)$$

In Eq. (12), N_x represents the normal force; M^c is the bending moment, similar to classical beam theory; M^s is the higher-order moment associated with shear deformation; and Q is the shear force. These quantities are calculated by properly integrating the stresses that occur across the beam thickness.

$$\begin{pmatrix} N_x \\ M^c \\ M^s \\ Q \end{pmatrix} = b \int_{-\frac{h}{2}}^{\frac{h}{2}} \begin{pmatrix} \sigma_x^k \\ \sigma_x^k z \\ \sigma_x^k f \\ \tau_{zx}^k f' \end{pmatrix} dz = \begin{bmatrix} A & B & C & 0 \\ B & D & E & 0 \\ C & E & F & 0 \\ 0 & 0 & 0 & H \end{bmatrix} \begin{pmatrix} \varepsilon_x^0 \\ k_x^b \\ k_x^s \\ \gamma_{zx}^0 \end{pmatrix}. \quad (12)$$

The matrices A, B, C, D, E, F , and H are defined in Eq. (13). These matrices represent the properties and geometry of the beam.

$$(A, B, C, D, E, F) = b \int_{-\frac{h}{2}}^{\frac{h}{2}} E^k(z) (1, z, f, z^2, fz, f^2) dz, \quad H = b \int_{-\frac{h}{2}}^{\frac{h}{2}} G^k(z) g^2 dz. \quad (13)$$

The change in potential energy (δV) due to the load q and the axial load N_0 is expressed in Eq. (14):

$$\delta V = \int_0^L \left(q \delta w + N_0 \frac{dw}{dx} \frac{d\delta w}{dx} \right) dx. \quad (14)$$

The change in kinetic energy (δK) is obtained using Eq. (15):

$$\begin{aligned} \delta K &= \int_0^L \int_{-b/2}^{b/2} \int_{-h/2}^{h/2} \rho(z) \left(\frac{d^2 u}{dt^2} \delta u + \frac{d^2 w}{dt^2} \delta w \right) dz dy dx \\ &= \int_0^L \left(I_A \frac{d^2 u_0}{dt^2} - I_B \frac{d^3 w_0}{dx dt^2} + I_C \frac{d^2 \phi}{dt^2} \right) \delta u_0 dx + \int_0^L \left(-I_B \frac{d^2 u_0}{dt^2} + I_D \frac{d^3 w_0}{dx dt^2} - I_E \frac{d^2 \phi}{dt^2} \right) \frac{d\delta w_0}{dx} dx \\ &+ \int_0^L \left(I_C \frac{d^2 u_0}{dt^2} - I_E \frac{d^3 w_0}{dx dt^2} + I_F \frac{d^2 \phi}{dt^2} \right) \delta \phi dx + \int_0^L I_A \frac{d^2 w_0}{dt^2} \delta w_0 dx. \end{aligned} \quad (15)$$

The moment of inertia coefficients $I_A, I_B, I_C, I_D, I_E, I_F$ are defined in Eq. (16):

$$(I_A, I_B, I_C, I_D, I_E, I_F) = b \int_{-\frac{h}{2}}^{\frac{h}{2}} \rho^k(z) (1, z, f, z^2, fz, f^2) dz. \quad (16)$$

The equations of motion are obtained by summing the coefficients $\delta u_0, \delta w_0$, and $\delta \phi_0$ and setting them equal to zero. This is done by integrating Eq. (10) using partial integration:

$$\begin{aligned} \frac{dN_x}{dx} &= I_A \frac{d^2 u_0}{dt^2} - I_B \frac{d^3 w_0}{dx dt^2} + I_C \frac{d^2 \phi}{dt^2}, \\ \frac{d^2 M^c}{dx^2} &= -q + N_0 \frac{d^2 w_0}{dx^2} + I_B \frac{d^3 u_0}{dx dt^2} - I_D \frac{d^4 w_0}{dx^2 dt^2} + I_A \frac{d^2 w_0}{dt^2} + I_E \frac{d^3 \phi}{dx dt^2}, \\ \frac{dM^s}{dx} - Q &= I_C \frac{d^2 u_0}{dt^2} - I_E \frac{d^3 w_0}{dx dt^2} + I_F \frac{d^2 \phi}{dt^2}. \end{aligned} \quad (17)$$

By substituting the stress results (N_x, M^c, M^s, Q) from Eq. (12) into Eq. (17), the following equations of motion can be obtained in terms of the unknown displacement variables (u_0, w_0, ϕ):

$$\begin{aligned} A \frac{d^2 u_0}{dx^2} - B \frac{d^3 w_0}{dx^3} + C \frac{d^2 \phi}{dx^2} &= I_A \frac{d^2 u_0}{dt^2} - I_B \frac{d^3 w_0}{dx dt^2} + I_C \frac{d^2 \phi}{dt^2}, \\ B \frac{d^3 u_0}{dx^3} - D \frac{d^4 w_0}{dx^4} + E \frac{d^3 \phi}{dx^3} &= -q + N_0 \frac{d^2 w_0}{dx^2} + I_B \frac{d^3 u_0}{dx dt^2} - I_D \frac{d^4 w_0}{dx^2 dt^2} + I_A \frac{d^2 w_0}{dt^2} + I_E \frac{d^3 \phi}{dx dt^2}, \\ A \frac{d^2 u_0}{dx^2} - B \frac{d^3 w_0}{dx^3} + C \frac{d^2 \phi}{dx^2} &= I_A \frac{d^2 u_0}{dt^2} - I_B \frac{d^3 w_0}{dx dt^2} + I_C \frac{d^2 \phi}{dt^2}, \end{aligned} \quad (18)$$

The solution of the equation of motion for the bending and free vibration analysis of a simply supported functionally graded sandwich beam is obtained using the Navier method. The boundary conditions for the simply supported beam are given in Eq. (19):

$$w_0 = N_x = M^c = M^s = 0, \quad x = 0 \text{ ve } x = L. \tag{19}$$

It is assumed that the solution takes the form given in Eq. (20):

$$\begin{aligned} u_0(x, t) &= \sum_{m=1,3,5}^{\infty} u_m \cos(\alpha x) e^{iat}, \\ w_0(x, t) &= \sum_{m=1,3,5}^{\infty} w_m \sin(\alpha x) e^{iat}, \\ \phi(x, t) &= \sum_{m=1,3,5}^{\infty} \phi_m \cos(\alpha x) e^{iat}. \end{aligned} \tag{20}$$

It is assumed that the uniform transverse load q acting on the upper surface of the beam is as given in Eq. (21):

$$q(x) = \sum_{m=1,3,5}^{\infty} Q_m \sin(\alpha x), \quad Q_m = \frac{4q_0}{m\pi}. \tag{21}$$

The analytical solution can be obtained from Eq. (22):

$$\begin{bmatrix} A\alpha^2 & -B\alpha^3 & C\alpha^2 \\ -B\alpha^3 & D\alpha^4 & -E\alpha^3 \\ C\alpha^2 & -E\alpha^3 & F\alpha^2 + H \end{bmatrix} \times \begin{Bmatrix} u_m \\ w_m \\ \phi_m \end{Bmatrix} = \begin{Bmatrix} 0 \\ Q_m \\ 0 \end{Bmatrix}. \tag{22}$$

The vertical displacement values of the FG porous sandwich beam are obtained by solving Eq. (22).

3. Results

In this study, the static analysis of TPMS-core functionally graded porous sandwich beams was performed. Effective material properties were defined using the mixture rule with an exponential variation, and equations of motion were derived via Hamilton’s principle. Upon analyzing Fig. 2:

- Figure 2a illustrates the vertical displacement (w) values versus the x/L ratio for three-layer types (1-8-1, 1-2-1, and 2-1-2) at $L/h = 5$. The 1-8-1 layer shows the lowest displacement, indicating higher rigidity, while the 2-1-2 layer exhibits the highest displacement, suggesting greater flexibility. Maximum displacement occurs at $x/L = 0.5$ and decreases toward the edges.
- Figure 2b presents w values for the 1-2-1 layer at $L/h = 5$ under conditions B1, B2, and B3. B1 shows the lowest displacement, indicating higher rigidity, while B3 exhibits the highest displacement, reflecting greater flexibility.
- Figure 2c shows the vertical displacement for the 2-1-2 layer at $L/h = 5$ and $L/h = 20$. The highest displacements occur at $L/h = 5$, with maximum deformation at $x/L = 0.5$ in all cases.

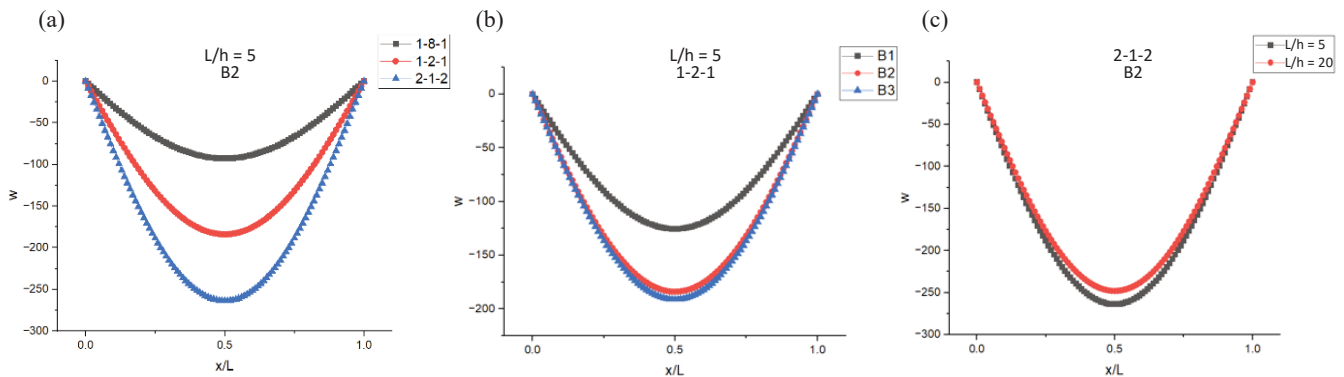


Fig. 2. (a) The vertical displacement values vary with the x/L ratio for three different layers at $L/h = 5$ ratio and B2; (b) the vertical displacement values vary with the x/L ratio for the 1-2-1 layer under B1, B2, and B3 conditions at $L/h = 5$ ratio; (c) the vertical displacement values vary with the x/L ratio for the 2-1-2 layer at $L/h = 5$ and $L/h = 20$ ratios at B2.

4. Conclusion

The static analysis of TPMS-core functionally graded porous sandwich beams provided key insights into material behavior under different conditions. The 1-8-1 layer showed the least vertical displacement, indicating high rigidity, while the 1-2-1 and 2-1-2 layers exhibited greater flexibility. The study also highlighted how varying density (B1, B2, B3) influenced deformation, underscoring the importance of structural design in optimizing performance. These findings are valuable for the application of TPMS-based sandwich structures in lightweight, high-performance materials. In future studies, diamond, split-P, primitive, neovius, and lidinoid TPMS types will also be considered.

Data availability statement

All data are available in the article.

Acknowledgment

The publication costs of this article were partially covered by the Estonian Academy of Sciences.

References

- Al-Ketan, O., Abu Al-Rub, R. K. 2021. MSLattice: a free software for generating uniform and graded lattices based on triply periodic minimal surfaces. *Mat. Design Process. Comm.*, **3**(6), e205. <https://doi.org/10.1002/mdp2.205>
- Demirhan, P. A. and Taskin, V. 2019. Bending and free vibration analysis of Levy-type porous functionally graded plate using state space approach. *Compos. B: Eng.*, **160**, 661–676. <https://doi.org/10.1016/j.compositesb.2018.12.020>
- Ejeh, C. J., Barsoum, I. and Abu Al-Rub, R. K. 2022. Flexural properties of functionally graded additively manufactured AlSi10Mg TPMS latticed-beams. *Int. J. Mech. Sci.*, **223**, 107293. <https://doi.org/10.1016/j.ijmecsci.2022.107293>
- Kurup, M. and Pitchaimani, J. 2023. Aeroelastic flutter of triply periodic minimal surface (TPMS) beams. *Compos. C: Open Access*, **10**, 100349. <https://doi.org/10.1016/j.jcomc.2023.100349>
- Lin, C., Wen, G., Yin, H., Wang, Z.-P., Liu, J. and Xie, Y. M. 2022. Revealing the sound insulation capacities of TPMS sandwich panels. *J. Sound Vib.*, **540**, 117303. <https://doi.org/10.1016/j.jsv.2022.117303>
- Nguyen-Xuan, H., Tran, K. Q., Thai, C. H. and Lee, J. 2023. Modelling of functionally graded triply periodic minimal surface (FG-TPMS) plates. *Compos. Struct.*, **315**, 116981. <https://doi.org/10.1016/j.compstruct.2023.116981>
- Qiu, N., Ding, Y., Guo, J. and Fang, J. 2025. Energy dissipation of sand-filled TPMS lattices under cyclic loading. *Thin-Walled Struct.*, **209**, 112848. <https://doi.org/10.1016/j.tws.2024.112848>
- Tran, K. Q., Hoang, T.-D., Lee, J. and Nguyen-Xuan, H. 2024. Three novel computational modeling frameworks of 3D-printed graphene platelets reinforced functionally graded triply periodic minimal surface (GPLR-FG-TPMS) plates. *Appl. Math. Model.*, **126**, 667–697. <https://doi.org/10.1016/j.apm.2023.10.043>
- Viet, N. V., Karathanasopoulos, N. and Zaki, W. 2022. Mechanical attributes and wave propagation characteristics of TPMS lattice structures. *Mech. Mater.*, **172**, 104363. <https://doi.org/10.1016/j.mechmat.2022.104363>

TPMS-südamikuga funktsionaalgradientstruktuuriga poorsete sandwich-talade staatiliste omaduste uurimine

Caner Solar, Pinar Aydan Demirhan ja Vedat Taskin

Funktsionaalgradientmaterjalid on uudsed struktuurid, mille loomiseks kombineeritakse erinevate materjalide omadusi. Funktsionaalgradientmaterjalide pooride suurus, kuju, jaotus ja tihedus muutuvad järk-järgult kindlas suunas, tagades kerguse ja energia neeldumise. Minimaalse energiaga kolmikperioodilise pinnaga (TPMS) struktuurid optimeerivad koormuse jaotumise ja energia neelamise omadusi, eriti kui neid kasutatakse sisekihtides. Uuringus teostati kinnistamata funktsionaalgradientstruktuuriga poorse sandwich-tala paindekatsed. Tala väliskihid olid isotroopsest materjalist, sisekiht TPMS-funktsionaalgradientstruktuuriga. Eeldati, et funktsionaalgradientstruktuuriga poorsete välis- ja sisekihtide omadused varieeruvad mööda ristlõiget vastavalt koormuse jaotumisele sõltuvalt kaugusest. Tala liikumise võrrandid tuletati Hamiltoni põhimõtte abil. Lahendid saadi lõplikul kujul Navier' meetodi põhjal. Arvutuslikud tulemused saadi, muutes suhtelist tihedust ja mahuosa, paksuse-pikkuse suhet ning sise- ja väliskihi paksuste suhet.